Solar Energy Materials & Solar Cells 222 (2021) 110921

Contents lists available at ScienceDirect

Solar Energy Materials and Solar Cells

journal homepage: www.elsevier.com/locate/solmat

Design of electrotunable all-weather smart windows

Ashish K. Chowdhary *, Debabrata Sikdar[1]

Department of Electronics and Electrical Engineering, Indian Institute of Technology Guwahati, Guwahati, Assam, 781039, India

ARTICLE INFO

Keywords:
Electro-optic
Fabry–Perot cavity
Infrared
Transfer matrix method
Transmission line method
Visible

ABSTRACT

Smart windows, capable of selective filtering of solar spectral radiation can help to significantly reduce the energy consumption by heating and cooling systems. However, robust and industry-standard designs of such windows, tunable for all-weather conditions, have been a challenge to date. In this work, we report on the design of ultra-thin electrotunable smart window 'glasses' using noble metals as well as their relatively-inexpensive alternatives. We adopt a lithography-free design approach using multilayer metallo-dielectric structure, that can dynamically control the intensity of transmitted solar radiation, depending upon the weather/climate condition. We make use of an electro-optic polymer as dielectric, which on applying voltage, changes the effective refractive index by virtue of electro-optic effect, allowing tunable filtering of visible and infrared radiation over a voltage range of −15 V to +15 V. Our theoretical results are in excellent agreement with those of full-wave simulations. Our design is robust, ultra-thin (60–100 nm thick), large-area compatible, polarization-independent, and angle-insensitive (up to 75 degrees). Aluminium oxynitride based glasses are suitable for designing military-grade, bulletproof, portable, and blast-resistant windows. The figure-of-merit calculations reveal that our relatively-inexpensive metals can outperform industry-standard commercial glasses as well as infrared-blocking plasmonic glasses, reported in the literature.

1. Introduction

Excessive consumption of fossil fuels in air-conditioning systems has been a primary contributor towards greenhouse gas emission leading to global warming [1]. For instance, in the U.S., heating and cooling systems alone consume 48% of the residential building energy [2]. Also, the air-conditioning systems installed in passenger vehicles increase fuel consumption by 25% [3]. Moreover, geographical locations with extreme weather conditions can adversely impact the efficiency of air-conditioning systems [4–6]. A smart window, capable of selective filtering of solar spectral radiation, can significantly reduce the energy consumption by heating and cooling systems, not only for residential buildings but also for state-of-the-art passenger vehicles [7–10].

In the present scenario, both passive and tunable windows are used globally. Considering passive windows, a design with multilayer-coated film over the window glass [5–7] or nanoparticles embedded inside the glass matrix [11] can help in blocking the undesired IR radiation transmission. However, the designs of such window glasses reported to date either do not possess industry-standard figure-of-merit or have complex fabrication process [8–10]. Moreover, static windows once fabricated, cannot be tuned to our specific needs. Considering switchable windows, tunability can be achieved by applying either external thermal or electrical energy. For thermal tuning, phase change materials such as vanadium oxide (VO_2) [12] and Ge2Sb2Te5 (GST225) [13] can be used. For electrical tuning, electro-optic (EO) polymer [14,15], epsilon-near-zero (ENZ) material [16,17], liquid and organic crystals [18], graphene [19], and n-type indium antimonide (n-InSb) [20] can be used. Recently, smart windows based on nanocomposite [21] and hydrogel [22] have also been reported. Even though a few electrochromic glasses were reported [23–26], the design of smart glasses for controlled transmission of solar radiation as per dynamic weather conditions, remained unexplored. In addition, production cost and longevity of switchable glasses reported to date, limit their commercial use on a large scale [27].

To bridge that gap in the literature, here, we propose design of ultra-thin electrotunable smart window glasses for dynamic control of transmitted solar radiation as per our convenience. To keep our design simple, we use **multilayer metallo-dielectric** (MLMD) planar structure, where a dielectric layer is inserted between the two metallic layers and the top and bottom metallic layers are kept identical throughout. We use noble metals [gold (Au) and silver (Ag)] as well as alternative materials [copper (Cu), indium tin oxide (ITO), aluminium-doped zinc oxide (AZO), and aluminium oxynitride (ALON)] as metallic layers, and an EO polymer, 4-dimethyl-amino-N-methyl-4-stilbazoliumtosylate

* Corresponding author.
E-mail addresses: ashis176302003@iitg.ac.in (A.K. Chowdhary), deb.sikdar@iitg.ac.in (D. Sikdar).

[1] D. Sikdar acknowledges the support from PROJ. NO. xEEESUGIITG01218xxDS001 funded by IIT GUWAHATI.

https://doi.org/10.1016/j.solmat.2020.110921
Received 7 September 2020; Received in revised form 7 December 2020; Accepted 8 December 2020
Available online 15 December 2020
0927-0248/

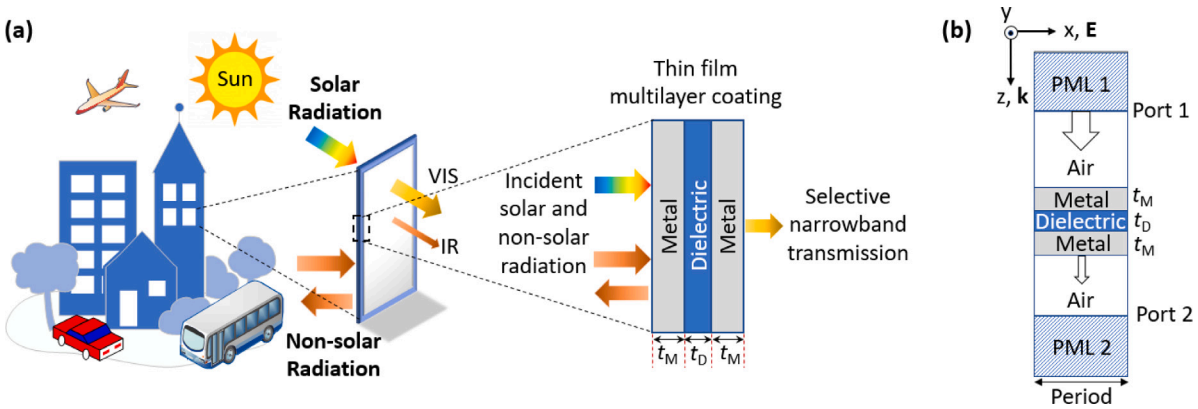

Fig. 1. Artistic outlook depicting a hot weather condition showing (a) 3D side view of our multilayer metallo-dielectric window glass, capable of selective filtering of visible (VIS) and infrared (IR) radiation, reflecting non-solar radiations coming from the heated objects (streets, vehicles, and nearby buildings) in mid-wave and long-wave infrared wavelength regime, and (b) 2D simulation model showing a unit cell. The incident radiation from port 1 is a plane wave of transverse magnetic (TM) polarization travelling along the z-direction. The reflection and transmission coefficients are calculated using S parameters obtained from full-wave simulations. A couple of perfectly matched layers (PML) are deployed at the top and bottom of the unit cell to avoid undue reflections arising due to confinement of the simulation domain. Note that the thickness of metallic layers at the top and bottom (t_M) and dielectric (t_D) may vary depending upon the type of materials used.

(DAST), as dielectric layer. A bias voltage ranging from −15 V to +15 V is used to achieve tunable filtering of solar radiation, spanning over 400–1800 nm, including visible (VIS; 400–750 nm), near-infrared (NIR; 750–1000 nm), and a part of short-wave infrared (SWIR; 1000–1800 nm) wavelengths. Besides, our MLMD glasses offer very high reflection to the non-solar radiation spectrum [28]; reflecting over 90% of incident radiation spanning over 3–30 μm, including mid-wave infrared (MWIR; 3–8 μm), long-wave infrared (LWIR; 8–15 μm), and a part of far-infrared (FIR; 15–30 μm) wavelengths. Our theoretical results obtained using transfer matrix method (TMM), transmission line method (TLM), and Fabry–Perot interferometer (FPI) technique agree well with those of finite element method (FEM) based full-wave simulations which validates our results [29,30]. Our smart glasses can be integrated into advertising screens, electronic curtains, room partitions, skylights panels, etc. Aluminium oxynitride based glasses can be used in fighter aircraft, military vehicles, high security buildings, and submarine applications.

物理原理

2. Physical principles of controlling solar radiation

The sun's solar radiation spectral regime lies mostly in visible, NIR, and SWIR wavelengths. Of the total solar irradiance, 53% is contributed by the IR regime, whereas, a significant 44% is contributed by the visible regime [11]. Radiative heating inside a room can be contributed by both solar as well as non-solar radiation [6–8]. An artistic view of our MLMD based smart window for a hot weather condition is shown in Fig. 1(a). On a hot day, the non-solar radiation comes from the heated objects (streets, vehicles, and nearby buildings) in MWIR and LWIR wavelength regime [31]. For hot weather condition, when illumination is desirable inside the room, ideally, a window should allow transmission of visible radiation and block the transmission of IR radiation [6,7,9]. Whereas, for cold weather, the transmission of both visible and IR radiation becomes desirable. While the majority of the works reported so far on smart windows are designed for hot weather condition [8–11,23–25], we report solutions suitable for all-weather conditions.

As per the dynamic weather condition, our window can either allow or block solar radiation, selectively. Here, we introduce four possible modes of operation, namely, 'Bright and Cool' (BC) mode (allowing visible but blocking IR), 'Bright and Warm' (BW) mode (allowing both visible and IR), 'Dark and Warm' (DW) mode (blocking visible but allowing IR), and 'Dark and Cool' (DC) mode (blocking both visible and IR). During hot weather, BC and DC modes are useful when radiative heating of a cold room becomes undesirable. On the contrary, during cold weather, BW and DW modes are convenient when radiative heating of a cold room is desirable to maintain ambient room temperature. Moreover, by filtering visible radiation, these smart windows can also control indoor illumination to ensure sufficient visible light transmission useful for day-to-day activities [16]. We found that DC mode is more suitable in specific applications such as mounting smart glasses on the rooftop of cold storage buildings for radiative cooling (by reflecting both visible and IR radiation) or on top of solar cell panels to increase their absorption efficiency (by absorbing both visible and IR radiation), hence, we addressed them separately in our previous work [32].

1 BC
2 BW
3 DW
4 DC

3. Simulation and theoretical modelling

仿真和理论建模

3.1. Design and working principle

A two-dimensional model of unit cell under consideration is shown in Fig. 1(b). Our MLMD structure can be approximated as a Fabry–Perot cavity, where the top and bottom metallic layers represent lossy mirrors and the dielectric layer can be considered as a resonator cavity. The corresponding condition of resonance wavelength is represented by [33]:

$$2Kn_D t_D + 2\phi = 2\pi m \quad (1)$$

where $K = 2\pi/\lambda_0$ is the wavevector, λ_0 is the resonance wavelength of the resonator cavity, n_D is the refractive index, t_D represents the thickness of the dielectric, ϕ represents the phase shift after reflection from the two metallic layers, and m is integer, representing the order of resonance inside MLMD cavity.

We use finite element method (FEM) solver of the COMSOL Multiphysics: ray optics module to simulate absorption, reflection, and transmission spectra over the solar (400–1800 nm) and non-solar (3–30 μm) spectral regime, shown in Fig. 2(a) and 2(b). We considered an incident plane wave of TM polarization for simulation. For the MLMD structure we assumed gold as a material for the top and bottom metallic layers, each being 5 nm thick, and a dielectric layer with thickness, t_D = 50 nm, of a material having a refractive index, $n_D = 2.2$. The optical constants of the materials used in this work are taken from [16,34–36]. To obtain accurate results, we deployed wavelength domain solver with physics-controlled extra-fine meshing, where the maximum and the minimum allowed mesh element sizes are 21.4 nm and ~ 0.1 nm, respectively, to be able to effectively model all structural detail. Each air layer (at the top and bottom) is considered to be 400 nm thick.

过渡反射

To avoid undue reflections, arising due to confinement of the simulation domain, perfectly matched layers (PML) of 200 nm thickness

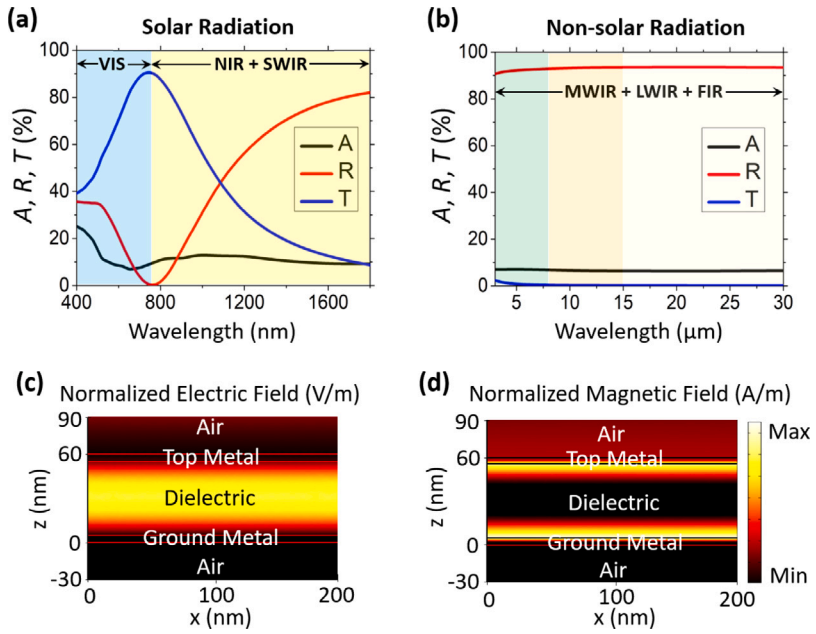

Fig. 2. Numerically calculated absorption, reflection, and transmission spectra for multilayer metallo-dielectric glass for both (a) solar and (b) non-solar radiation spectra, taking top and bottom metallic layers (t_M) as gold, each being 5 nm thick, and dielectric with thickness, t_D = 50 nm and refractive index, n_D = 2.2. For our study, the solar radiation spectra span over 400–1800 nm, including visible (VIS; 400–750 nm), near-infrared (NIR; 750–1000 nm), and a part of short-wave infrared (SWIR; 1000–1800 nm) wavelengths. The non-solar radiation spectra span over 3–30 μm, including mid-wave infrared (MWIR; 3–8 μm), long-wave infrared (LWIR; 8–15 μm), and a part of far-infrared (FIR; 15–30 μm) wavelengths. The presence of resonance mode is depicted by magnitude of (c) normalized electric field (**E**), and (d) normalized magnetic field (**H**) distribution, corresponding to the resonance wavelength (λ_0 = 750 nm).

are used at the top and bottom of the unit cell. Periodicity of the unit cell along both lateral directions is taken to be 200 nm, implemented using Floquet boundary condition. The plane wave excitation is applied at port 1, which acts as 'source' whereas port 2 acts as a 'destination'. The overall transmission (T) and reflection (R) in percentage are obtained using the following equations: $T = 100 \times |S_{21}|^2$ and $R = 100 \times |S_{11}|^2$, where S_{21} and S_{11} are the scattering (S) parameters calculated numerically by the FEM solver, for the two-port network system deployed here, over the wavelength range of interest. Using the equation: $A = 100 - R - T$, absorbance (A) in percentage can be further calculated. The normalized electric (**E**) and magnetic (**H**) field distribution corresponding to the resonant wavelength, depicted in Fig. 2(c) and 2(d), clearly show the existence of resonant mode confined inside the dielectric layer. As we consider metal layer thickness less than the skin depth [37], the enhanced transmission is achieved at resonance condition since the supported resonant modes are leaky and can couple with the incident and transmitted electromagnetic radiation.

3.2. Theoretical analysis 理论分析

To support our simulation results, we apply transfer matrix method (TMM), transmission line method (TLM), and Fabry–Perot interferometer (FPI) technique. Here, we take top and bottom metallic layers as silver, each being 5 nm thick, and dielectric with thickness, t_D = 60 nm and refractive index, n_D = 2.2. For TMM case, we consider five layers and four interfaces, assuming a plane wave of linear polarization falling on top of our multilayered glass, as shown in Fig. 3(a). Here, n, Y, and t represent the refractive index, admittance, and thickness of the corresponding layer, respectively. We assume medium to be linear, non-magnetic, and homogeneous [33]. The transmission spectra obtained using TMM is shown in Fig. 3(d).

For TLM, a simplified circuit model is shown in Fig. 3(b). Here, Z, k, and t are characteristic impedance, propagation constant, and the thickness of the transmission line, respectively, corresponding to the identical (top and bottom) metallic and dielectric layers. The input impedance at interfaces 3 and 2 seen from the top towards the bottom, can be obtained using [14,37]:

$$Z_{in,3} = Z_M \frac{Z_0 - jZ_M \tan(k_M t_M)}{Z_M - jZ_0 \tan(k_M t_M)} \quad (2a)$$

$$Z_{in,2} = Z_D \frac{Z_{in,3} - jZ_D \tan(k_D t_D)}{Z_D - jZ_{in,3} \tan(k_D t_D)} \quad (2b)$$

where Z_0 is free space impedance of air. The corresponding reflection coefficients at metal–dielectric interfaces are:

$$r_3 = \frac{Z_{in,3} - Z_D}{Z_{in,3} + Z_D} = |r_3| \angle \phi_3 \quad (3a)$$

$$r_2 = \frac{Z_{in,2} - Z_D}{Z_{in,2} + Z_D} = |r_2| \angle \phi_2 \quad (3b)$$

Here, ϕ_3 and ϕ_2 denote the phase shift upon reflection at metal–dielectric interfaces 3 and 2, respectively. The accumulated round trip phase ($\phi_3 + \phi_2$) upon reflection is shown in Fig. 3(d). When the accumulated round trip phase becomes zero, maximum transmission (T_{max}) is allowed at the resonant wavelength λ_0 = 750 nm [14].`

Next, we use FPI method to determine T_{max} corresponding to the resonant wavelength supported by the cavity [see Fig. 3(c)]. Here identical top and bottom metallic layers represent lossy mirrors and the dielectric layer can be considered as a resonator cavity medium. The condition for maximum transmission, given by Eq. (1), occurs in integral multiples of 2π as shown in Fig. 3(e).

A comparison among FEM, TMM, TLM, and FPI is shown in Fig. 3(d) and 3(e). An excellent agreement between simulation (FEM) and theory (TMM) is seen for the entire solar spectral regime. TLM allows us to accurately predict the resonant wavelength (λ_0 = 750 nm) when the accumulated round trip phase becomes zero. FPI technique accurately predicts the peak transmission (T_{max} = 97.2%) at the resonant wavelength (λ_0 = 750 nm), which exactly matches with TMM and FEM transmission peaks. Hence, a perfect match between simulation and theory, indeed, validates our findings. Under the results and discussion section, we will use TMM and FEM to compare theoretical and simulation results.

$$Z_{in,3} = Z_M \frac{Z_0 - jZ_M \tan(k_M t_M)}{Z_M - jZ_0 \tan(k_M t_M)} \qquad r_3 = \frac{Z_{in,3} - Z_D}{Z_{in,3} + Z_D} = |r_3|\angle\phi_3 \qquad 2Kn_D t_D + 2\phi = 2\pi m$$

$$Z_{in,2} = Z_D \frac{Z_{in,3} - jZ_D \tan(k_D t_D)}{Z_D - jZ_{in,3} \tan(k_D t_D)} \qquad r_2 = \frac{Z_{in,2} - Z_D}{Z_{in,2} + Z_D} = |r_2|\angle\phi_2 \qquad \text{where } K = 2\pi/\lambda_0$$

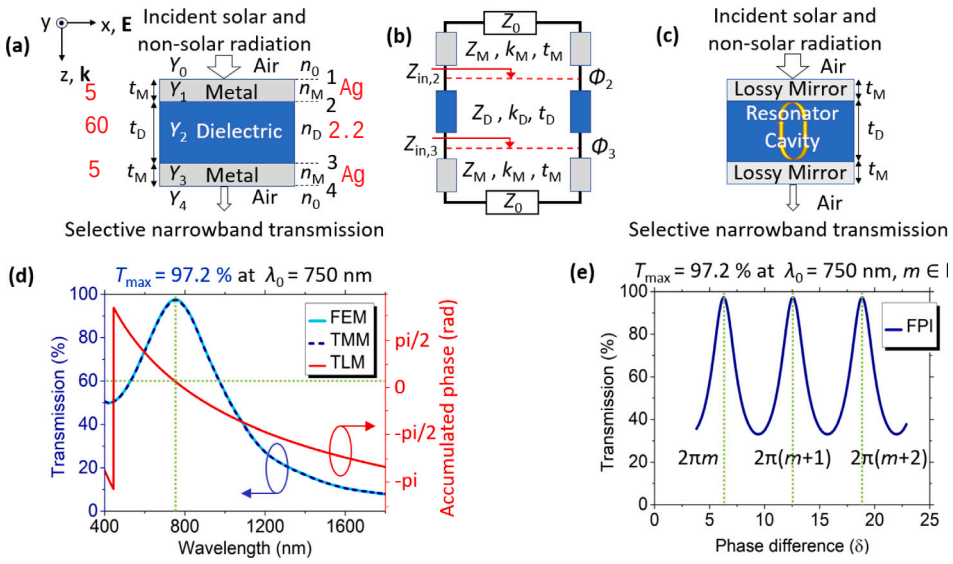

Fig. 3. Detailed schematic of the proposed design shown in Fig. 1, analysed using (a) transfer matrix method (TMM), (b) transmission line method (TLM), and (b) Fabry–Perot interferometer (FPI). For all three cases, we take metallic layers at the top and bottom as silver, each being 5 nm thick (t_M), and dielectric with thickness, t_D = 60 nm and refractive index, n_D = 2.2. In (a) Y and n represent the admittance and refractive index of the corresponding layer, respectively. In (b) Z_{in}, Z, k, and ϕ are input impedance, characteristic impedance, propagation constant, and phase shift upon reflection at the interface of the transmission line, respectively. (d) shows comparison between transmission spectra of finite element method (FEM; represented by a cyan solid line) and TMM (represented by a royal blue short dashed line). TLM (represented by a red solid line) accurately predicts the resonant wavelength (λ_0 = 750), when the accumulated round trip phase becomes zero (represented by green square dot cross lines). (e) FPI (represented by a royal blue solid line) accurately predicts the peak transmission (T_{max} = 97.2%; represented by green square dot cross lines) corresponding to the resonant wavelength which occurs in integral multiples of 2π, exactly matches with FEM and TMM transmission peak. (For interpretation of the references to colour in this figure legend, the reader is referred to the web version of this article.)

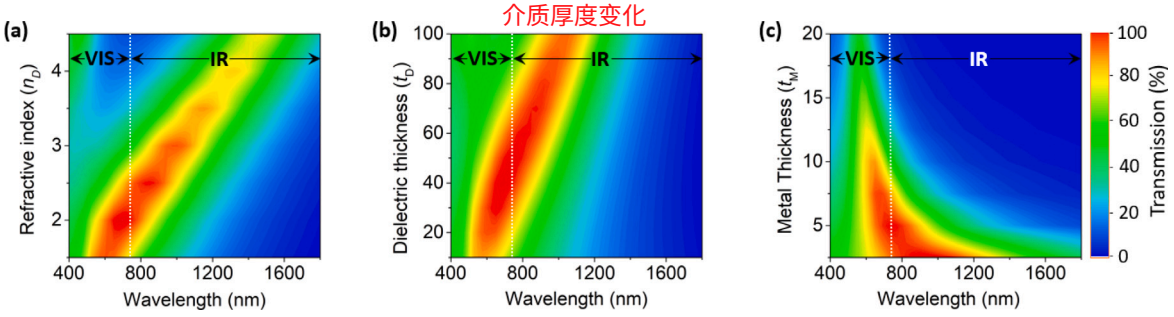

Fig. 4. Simulation based parametric study showing contour plot to optimize our MLMD glass design for varying (a) refractive index of dielectric layer, n_D (considering t_M = 5 nm and t_D = 50 nm), (b) thickness of dielectric layer, t_D (considering t_M = 5 nm and n_D = 2.2), and (c) thickness of top and bottom metallic layers, t_M (considering n_D = 2.2 and t_D = 50 nm). In each case, top and bottom metallic layers are chosen as gold (Au).

4. Results and discussion

4.1. Parametric analysis

理想的

To obtain a desirable optical response, we optimize the design of our MLMD glass by studying the effect of change in device dimensions. Fig. 4 shows the contour plot for varying refractive index (n_D) and thickness (t_D) of dielectric layer as well as varying thickness of metallic layers (t_M). For each of the cases, we consider top and bottom metallic layers as gold. Fig. 4(a) and 4(b) depict a redshift with increase in the dielectric refractive index (considering t_M = 5 nm and t_D = 50 nm) and dielectric thickness (considering t_M = 5 nm and n_D = 2.2), respectively, as predicted by Eq. (1). The reason can be attributed to the increases in the effective path length of electromagnetic waves with increase in refractive index/thickness of the medium, leading to slow propagation of wave inside, indicating, a mode with a larger resonant wavelength is supported by the cavity [38]. Fig. 4(c) depicts a dip in overall transmission spectra with increase in metal thickness (considering n_D = 2.2 and t_D = 50 nm). As per basic electromagnetic theory, the thicker the metal, the lesser will be the depth of penetration of electromagnetic waves through the structure [25]. However, in our case, to cover a larger spectrum of visible and IR radiation, metallic layers with lower thickness is desirable for a broadband response [14]. Therefore, for all our future designs, top and bottom metallic layers are chosen to be 5 nm thick. Also, to achieve transmission peak exactly at the desired resonance wavelength, the dielectric thickness is adjusted in each case (between 50 and 90 nm).

4.2. Electrotunable smart glasses

所需的 要么

To achieve transmission peak at the desired wavelength, either the refractive index (n_D) or the thickness (t_D) of dielectric needs to be changed. For example, to achieve maximum transmission in both visible and IR spectral regime (BW mode), 750 nm is the desired resonance wavelength for peak transmission. For this purpose, many different type of EO materials are mentioned in the literature [39]. The comparison among a few EO materials that may be considered for our smart window design is shown in Table 1. In this work, we choose DAST, an EO polymer having tunability near-visible regime. This polymer possesses a large EO coefficient (3.41 nm/V) that is desirable to attain maximum tunability with minimum bias voltage.

Table 1
Comparison among a few different EO materials that may be considered for our smart window design [39].

EO materials	$\frac{dn}{du}$ (nm/V)	IC compatibility	Remarks
$LiNbO_3$	0.160	No	High melting point (> 900 °C), limited bandwidth, and good stability.
Doped polymers	0.125	Yes	Good bandwidth but temperature sensitive.
DAST	3.410	Yes	High melting point (259 °C), large bandwidth, and good stability.

Note: $\frac{dn}{du}$: electro-optic (EO) coefficient.

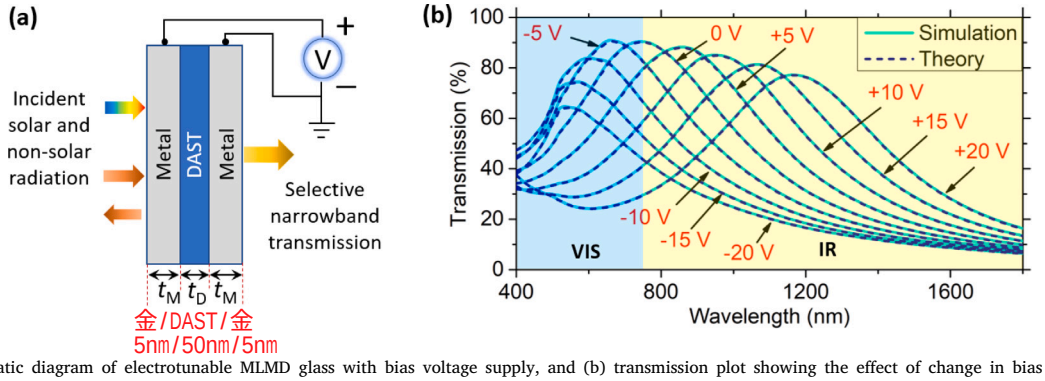

Fig. 5. (a) 2D schematic diagram of electrotunable MLMD glass with bias voltage supply, and (b) transmission plot showing the effect of change in bias voltage at arbitrarily chosen nine discrete values between −20 V and +20 V in steps of 5 V, considering top and bottom metal of gold, each 5 nm thick (t_M) and dielectric being DAST polymer, 50 nm thick (t_D).

The refractive index of DAST as a function of the applied voltage is given by [14]:

$$n_D = n_0 + \frac{dn}{du}\frac{V}{t_D} \quad (4)$$

折射率与施加电压关系

where $n_0 = 2.2$ is the refractive index of DAST polymer at zero bias, $\frac{dn}{du} = 3.41$ nm/V being EO coefficient with u being the applied electric field, V is the applied voltage, and t_D denotes the thickness of the DAST polymer. A two-dimensional schematic diagram of electrotunable MLMD glass with bias voltage supply is shown in Fig. 5(a). The transmission plot for a varying bias voltage is shown in Fig. 5(b) at arbitrarily chosen nine discrete values between −20 V and +20 V in steps of 5 V. Here, we considered the top and bottom metal layers as gold, each 5 nm thick and a 50 nm thick dielectric layer of DAST polymer.

In Fig. 5(b), it can be seen that between −20 V and +20 V, there is a gradual spectral shift in the transmission peak towards longer wavelengths. Choosing an appropriate bias voltage allows shifting the transmission peak entirely into either visible or IR region. Here, our idea is to set BW mode at zero bias (0 V) which allows both visible and IR transmission. Then we achieve BC and DW modes simply by shifting the transmission peak into either visible or IR regime, respectively. Ideally, with a larger applied potential, a larger shift in the transmission peak towards either visible or IR regime is expected. This will result in a larger transmission in one regime, e.g. either visible (at negative bias) or IR (at positive bias), along with a stronger blocking in the other regime. For a low-power design, considering symmetric positive and negative bias voltages, here we chose −15 V for BC mode and +15 V for DW mode, for demonstrating the proof-of-the concept. Note that there is a trade-off between a larger operating voltage and a mode's performance in selective filtering of radiation.

偏置电压 对称的

For our first three MLMD based window glass design, we choose top and bottom metallic layers both to be either Au or Ag or Cu and DAST polymer as dielectric layer, for all the three cases [see Fig. 6(a), 6(b), and 6(c)]. These electrotunable glasses can operate under BC, BW, and DW modes over a voltage range of −15 V to +15 V. For instance, considering Au–DAST–Au based glasses, when we apply a negative bias (−15 V) our smart window works in BC mode, useful during summer when maximum indoor illumination with minimum radiative heating is desired. Whereas, on applying a positive bias (+15 V) our window works in DW mode, useful during winter when minimum indoor illumination with maximum radiative heating is desired. By default (no bias applied i.e. 0 V) it works in BW mode, which is useful during winter when maximum indoor illumination with maximum radiative heating is desired.

透明导电氧化物

For a low-cost design, we further explore the use of transparent conductive oxides (TCOs) as metallic layers. Among the three TCOs considered, ALON is abundant, low-cost, toughest, and lightweight material [40], suitable for designing military-grade, bulletproof, portable, and blast-resistant windows [41]. On careful investigation, we observe that glasses based on ITO, AZO, and ALON can provide some unique optical response by applying a bias voltage across the DAST layer [see Fig. 6(d), 6(e), and 6(f)]. For example, ITO–DAST–ITO based glass on application of negative bias (−15 V), works in BW mode, allows over 88% of IR and over 83% visible transmission, desirable during winter. Whereas, on application of positive bias (+15 V), it works in BC mode, where ~75% visible and merely 45% IR radiation is transmitted—desirable during summer. If we can further increase the bias voltage (say +45 V), IR transmission falls below 20%. When no bias (0 V) is applied, we get an intermediate solution, useful during spring/autumn / rainy season when both indoor illumination and radiative heating is desired to some extent. Such excellent control over IR blocking capabilities makes MLMD glasses suitable for designing an all-weather smart window. Detailed specifications of our smart glasses are provided in Table 2.

车用级别 防弹 便携式 防爆 春/秋/雨

4.3. Polarization and angle study

To ensure that our design is suitable for daytime operation, we study both TM and TE polarization using Au–DAST–Au based design with a bias voltage of ±15 V. Fig. 7(a) shows that even after applying voltage over −15 V to +15 V, transmission spectra remain unaffected by change in polarization of the incident wave, hence, showing polarization-insensitivity. To account for the effect of dynamically changing position of the sun, we also study for varying angle of incidence, ranging over 0–85 degrees at 0 V bias. Fig. 7(b) and 7(c) show that our design is angle-insensitive up to 75 degrees of angle of incidence for both TM and TE cases, with over 90% transmission efficiency, hence, making our smart glasses a practical choice for daytime operation.

4.4. Figure of merit

To meet industry standards, we evaluate the performance of our electrotunable smart glasses, by calculating their figure of merit [5,7,9].

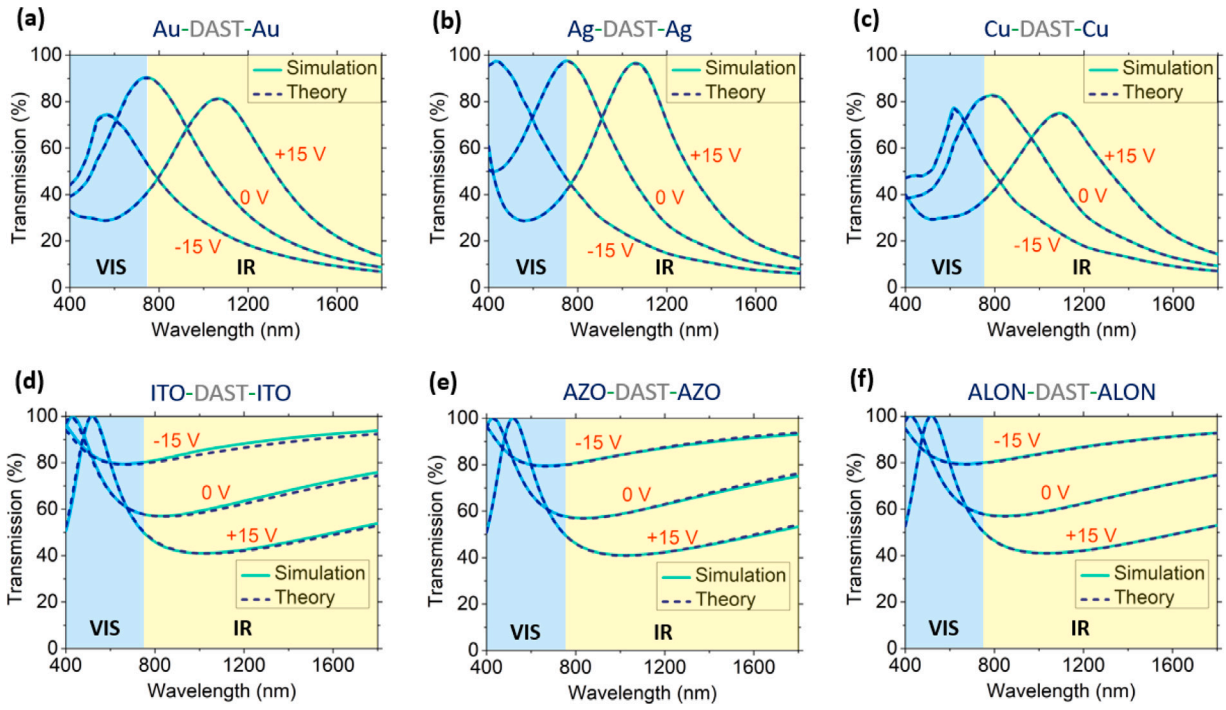

Fig. 6. Transmission spectra for our electrotunable smart glasses choosing top and bottom metallic layers, both made of either (a) gold, (b) silver, or (c) copper, and dielectric layer as DAST polymer in each case, with an applied bias voltage of −15 V, 0 V, and +15 V working in BC (Bright and Cool; useful in hot weather with illumination), BW (Bright and Warm; useful in cold weather with illumination), and DW (Dark and Warm; useful in cold weather without illumination) modes, respectively. Similarly, design with choice for metallic layers at top and bottom to be either (d) ITO, (e) AZO, or (f) ALON, and dielectric layer as DAST polymer in each case, with an applied bias voltage of −15 V, 0 V, and +15 V works in BW, intermediate (useful in autumn/spring with illumination), and BC modes, respectively.

Table 2
Detailed specifications of our electrotunable smart window glasses.

Structure (thickness in nm)	Mode of operation	Remarks
Au(5)–DAST(50)–Au(5)	BC, BW, DW	T_{peak} = 90.4%, ultra-compact, expensive.
Ag(5)–DAST(60)–Ag(5)	BC, BW, DW	T_{peak} = 97.5%, high tunability, less expensive compared to Au.
Cu(5)–DAST(60)–Cu(5)	BC, BW, DW	T_{peak} ~ 80.0%, relatively inexpensive compared to Au and Ag.
ITO(5)–DAST(90)–ITO(5)	BW, IMD, BC	$T_{IR,BW}$ = 88.3%, $T_{IR,BC}$ = 45.6%, relatively inexpensive.
AZO(5)–DAST(90)–AZO(5)	BW, IMD, BC	Performance same as ITO, relatively inexpensive.
ALON(5)–DAST(90)–ALON(5)	BW, IMD, BC	Performance same as ITO, cheapest, lightweight, and toughest.

Note: BC: Bright and Cool; BW: Bright and Warm; DW: Dark and Warm; IMD: intermediate; Mode of Operation at −15 V, 0 V, and +15 V power supply.

The three most commonly used parameters are visible transmittance (VT), infrared transmittance (IRT), and solar heat gain coefficient (SHGC), which represent the fraction of visible, infrared, and total solar radiation transmitted through a glass window over a particular range of wavelength, respectively [11]. A general mathematical representation is given by:

$$\mathrm{FOM} = \frac{\int_{\lambda_{\min}}^{\lambda_{\max}} I_{\mathrm{solar}}(\lambda) T(\lambda) \mathrm{d}\lambda}{\int_{\lambda_{\min}}^{\lambda_{\max}} I_{\mathrm{solar}}(\lambda) \mathrm{d}\lambda} \tag{5}$$

where $T(\lambda)$ and $I_{\mathrm{solar}}(\lambda)$ are considered to be wavelength dependent transmission and sun's solar irradiance at the sea level, respectively [11]. For simplifying the complex calculations, a spectra range between 400 and 1800 nm is considered, over which almost 90% solar radiation is received [8]. The spectral range of VT, IRT, and SHGC for our window glass design lies over 400–750 nm, 750–1800 nm, and 400–1800 nm, respectively.

An ideal window designed for hot weather condition should have VT value as high as possible and IRT value as low as possible. In contrast, for cold weather, both VT and IRT values should be as high as possible. For SHGC value calculation in BC mode over 400–1800 nm wavelength range, we take $T_{\mathrm{visible}}(\lambda) = 1$, and $T_{\mathrm{IR}}(\lambda) = 0$, which gives ideal SHGC value as 0.55. Similarly, for BW and DW modes within the same spectral regime, the ideal SHGC value comes out to be 1 and 0.45, respectively. VT, IRT, and SHGC ideal values are listed in Table 3.

Table 3
VT, IRT, and SHGC ideal values in different modes over solar radiation spectral range, $\lambda \in$ [400 nm, 1800 nm].

Mode of operation	VT	IRT	SHGC
BC mode	1	0	0.55
BW mode	1	1	1
DW mode	0	1	0.45

Note: BC: Bright and Cool; BW: Bright and Warm; DW: Dark and Warm; VT: Visible Transmittance; IRT: IR Transmittance; SHGC: Solar Heat Gain Coefficient.

Figure of merit calculations for BC, BW, and DW modes, comparing our MLMD based smart glasses with a few commercial glasses and previously reported infrared-blocking plasmonic glasses are shown in Fig. 8. A comparison of figure of merit for BC mode among our smart glasses and two double-pane argon low-emissivity coating commercial windows (CW I, and CW II), is shown in Fig. 8(a) [8–10]. In this case, our relatively inexpensive metals such as Ag, ITO, AZO, and ALON outperform industry-standard commercial window glasses.

Recently, Besteiro et al. designed thin-film plasmonic glasses to block IR radiations over 200–1700 nm spectral range [11]. Out of all the materials considered, their figure of merit calculation revealed

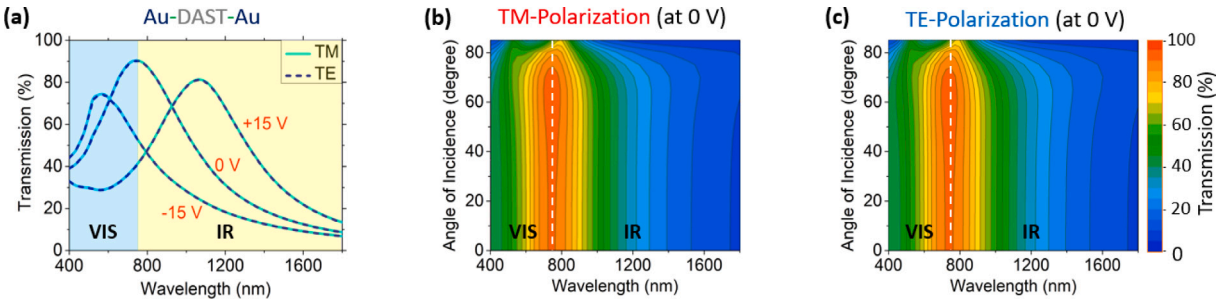

Fig. 7. Simulated transmission spectra showing (a) both TM and TE polarization for Au (5 nm)–DAST (50 nm)–Au (5 nm) structure under three modes of operation at −15 V, 0 V, and +15 V bias voltage, showing polarization insensitivity. Contour plot for angular transmission spectrum of the same structure at 0 V bias, showing over 90% transmission efficiency for a wide angle of incidence (up to 75 degrees) for both (b) TM and (c) TE polarization.

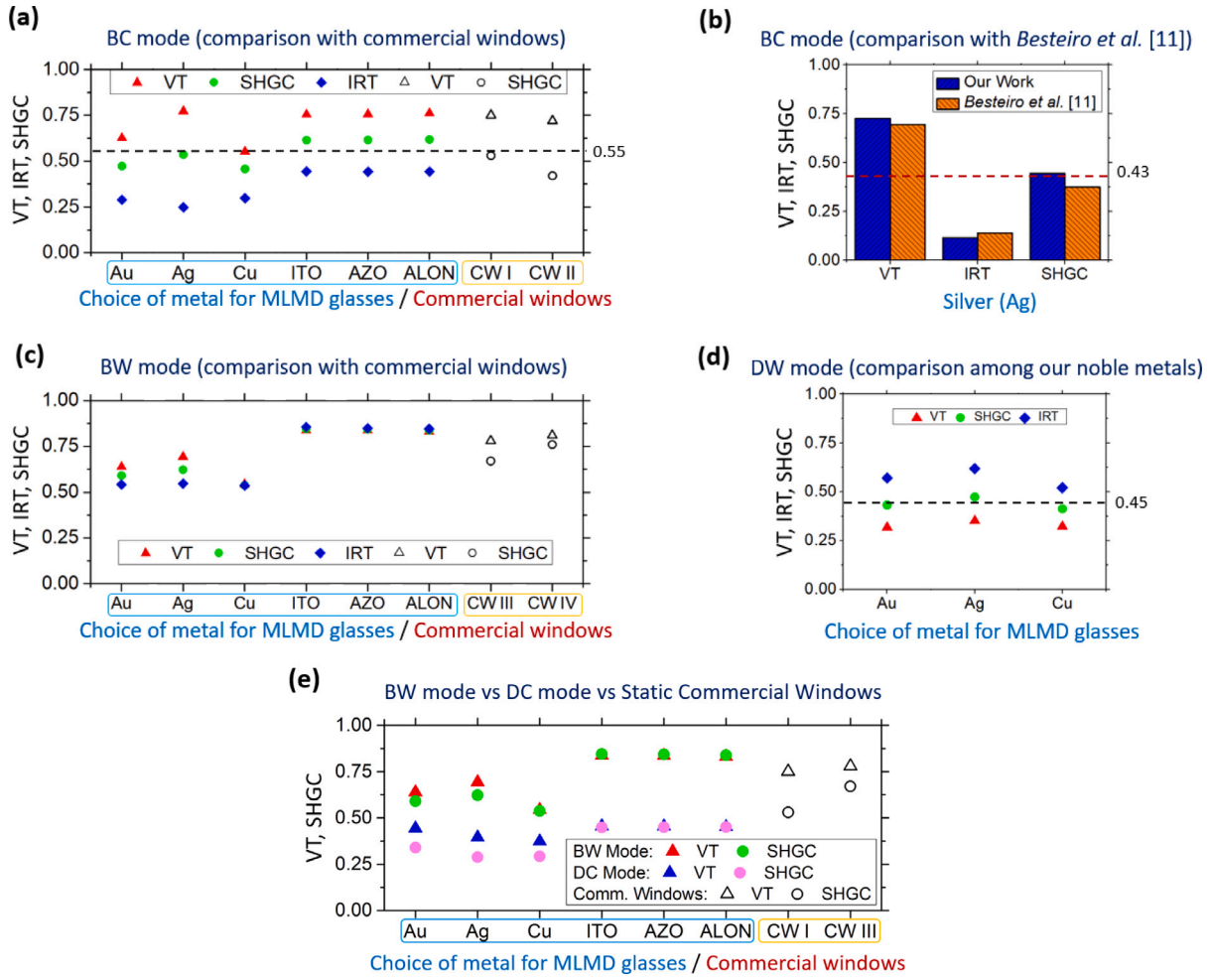

Fig. 8. Figure of merit representation for (a) BC mode, comparing our smart glasses with two commercial double-pane argon low-emissivity coating glasses (CW I and CW II) [8–10], (b) BC mode, comparison between our silver based smart glasses and silver nanoshell based IR-blocking plasmonic glasses [11], (c) BW mode, comparing our smart glasses with commercial double-glazed, high-solar-gain low-emissivity glass and double-pane clear glasses (CW III and CW IV) [9,10], (d) new DW mode, comparison among our gold, silver, and copper based smart glasses, and (e) comparison between BW and DC modes of our glasses and the static commercial windows (CW I and CW III). In each case, DAST polymer is used as dielectric layer. Note that in (a), (b), and (d) the short dashed horizontal lines represent the corresponding ideal SHGC value in each case.

that silver nanoshell based plasmonic glasses produced the best results. Fig. 8(b) shows a comparison between our silver based smart glasses and their silver nanoshell based plasmonic glasses. For a fair comparison, we take the mean value of their calculated and simulation data and optimized our design over the same spectral range (200–1700 nm) by considering 8 nm thick top and bottom silver layers alongside 95 nm thick DAST layer. For their spectral range, the calculated ideal SHGC value is 0.43. The figure of merit calculations reveals that our silver based smart glasses can outperform their silver nanoshell based plasmonic glasses in all the three parameters (VT, IRT, and SHGC).

A comparison among our smart glasses, commercial double-glazed high-solar-gain low-emissivity glass, and double-pane clear glass windows (CW III and CW IV) is shown in Fig. 8(c) [9,10]. In this case, our smart glasses based on relatively inexpensive metals such as ITO, AZO, and ALON outperform the industry-standard commercial window glasses. For the DW mode, a comparison among our Au-, Ag-, and Cu-based smart glasses is shown in see Fig. 8(d). In this case as well, silver

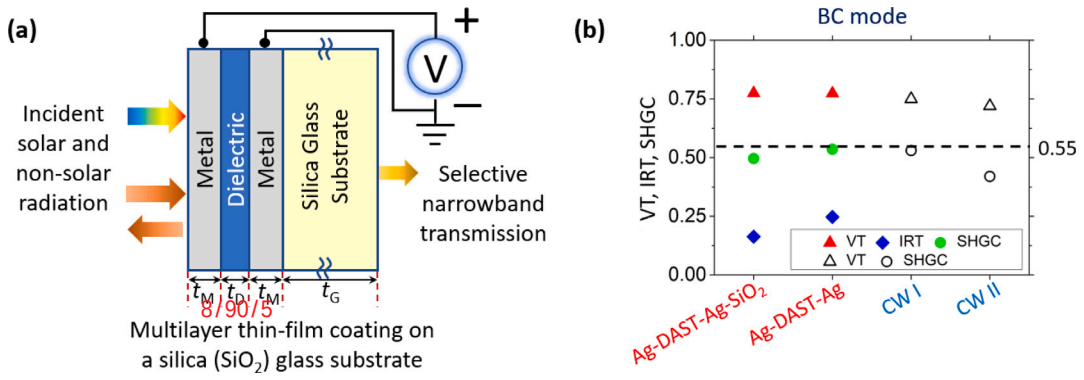

Fig. 9. (a) 2D schematic diagram (not to scale) of an electrotunable MLMD thin-film (with terminals for bias voltage supply) coated on optically-transparent silica (SiO_2) glass substrate. Here, the thicknesses of metal (t_M), dielectric (t_D), and silica glass substrate (t_G) are considered to be 8 nm, 90 nm, and 5 mm, respectively. (b) The figure of merit representation for BC mode showing a comparison among our Ag–DAST–Ag based smart glasses (with and without silica glass substrate) and a couple of commercial double-pane argon low-emissivity coating glasses (CW I and CW II) [8–10].

shows overall better performance compared to gold. Fig. 8(e) shows a comparison between the BW and DC modes of our glasses and the static commercial windows (CW I and CW III). Note that DC mode requires biasing of −30 V for Au, Ag, and Cu based designs and +50 V for ITO, AZO, and ALON based designs. The figure of merit calculation revealed that the overall performance of our relatively inexpensive metals (Ag, Cu, ITO, AZO, and ALON) is better compared to Au and also meets industry standards. Therefore, our MLMD based glasses could be a suitable choice for large scale commercial production of all-weather smart windows.

4.5. Effect of substrate

From a practical point-of-view, an ideal implementation of our MLMD film would be its integration with an insulated glass unit (IGU) used in buildings. This IGU will allow us to find out the rate of heat loss through a window, defined as U-value [8–10]. Therefore, it will be interesting to compare the performance of our MLMD glass, with and without an optically transparent silica (SiO_2) glass substrate. Fig. 9(a) shows a 2D schematic diagram of our electrotunable MLMD film (with bias voltage supply) coated on a silica glass substrate. Here, the thicknesses of the metallic layer (t_M), the dielectric layer (t_D), and silica glass substrate (t_G) are considered to be 8 nm, 90 nm, and 5 mm, respectively. Note that the thicknesses of metal and dielectric layers are manually optimized for coating on the glass substrate. To evaluate the performance, we calculate the figure-of-merit parameters in BC mode using Ag–DAST–Ag based glass. Fig. 9(b) shows a comparison of the VT, IRT, SHGC parameters obtained in BC mode among our Ag–DAST–Ag based smart glasses (with and without silica glass substrate) and a couple of commercial double-pane argon low-emissivity coating glasses (CW I and CW II) [8–10]. We observe that our proposed windows still exhibit overall better performance than the commercial windows when our MLMD glasses are coated on a single-pane glass substrate. Therefore, our MLMD based glasses could be a better and cheaper alternative to commercial double- or triple-pane low-emissivity glasses.

4.6. Prospective fabrication method and tolerance study

With the existing state-of-the-art nanoscale fabrication facilities, the fabrication of our proposed MLMD glass design is indeed feasible. For instance, Ag–DAST–Ag based MLMD glass can be fabricated by successive electron beam (e-beam) evaporation technique [39,42–44]. First, a silver metal layer of 5 nm thickness needs to be coated on the top surface of a two-sided polished silica glass substrate (typically 5 mm thick) using an e-beam evaporator [40]. Then a 60 nm thick DAST layer may be deposited as a single crystal over a large-area in a certain orientation on the top surface of the bottom silver layer. The graphoepitaxy technique may be used to control the orientation and solidification of the DAST crystals [39]. Finally, another 5 nm thick silver layer may be deposited at the top surface of DAST–Ag coating using the e-beam evaporation technique. For optical characterization, a microscope integrated with a spectrometer or a Fourier Transform Infrared (FT-IR) microscope and an electron multiplication charge-coupled device (CCD) camera may be used [42,43]. It is important to note that the optical response from such MLMD glasses is subjected to controlled environmental conditions during fabrication. However, fabrication imperfections may arise depending upon the deposition techniques employed and the surface smoothness of different materials used. Therefore, it is important to further analyse the effect of such imperfections on the design's performance.

Table 4 lists the results of the fabrication-tolerance study conducted for Ag–DAST–Ag based MLMD glass in BC, BW, and DW modes. Variations in VT, IRT, and SHGC values are shown over the solar radiation spectral regime with ±5% variation in thicknesses of top/bottom Ag layer (5 nm thick) and DAST layer (60 nm thick). We found that the performance parameters (VT, IRT, and SHGC) vary only marginally with ±5% variation in the thickness of each layer. This finding shows that our proposed MLMD glass designs are robust and the overall window performance is less prone to fabrication imperfections.

4.7. Application and future scope

Smart windows coated with our suggested MDLM based thin-film can be controlled via smart-home systems to provide security and privacy features alongside real-time tuning with only ±15 V supply. However, the major challenge lies in the durability of such electrotunable smart windows compared to ordinary windows. Since, TCOs are ENZ materials, their intrinsic properties may change when kept in direct contact with the DAST layer, across which voltage is applied [16]. To understand the effect of such undesirable change in ENZ material properties, we also study transmission spectra of our MLMD design by introducing a thin layer of SiO_2 (5 nm thick) sandwiched between top metal and middle DAST layer as well as bottom metal and middle DAST layer. Our simulation results reveal that the transmission spectra and overall performance remain unaffected by the introduction of thin SiO_2 layers, thus, making our design robust and durable.

Future work may include better optimization of structure using multiple metal–dielectric stacks and exploring more low-cost alternative materials. In this work, we have used DAST polymer as an EO material. This polymer possesses one of the largest EO coefficients among all those organic crystals available today [39]. DAST also has a large melting point (259 °C), a large electrical bandwidth, and exhibits stability up to 250 °C. Hence, it is expected that DAST based devices will be durable. As shown in Table 1, alternative EO materials such as

Table 4
Fabrication tolerance study for Ag–DAST–Ag based MLMD glass in BC, BW, and DW modes, showing variation in VT, IRT, and SHGC values over solar radiation spectral regime i.e. $\lambda \in$ [400 nm, 1800 nm], with ±5% variation in thicknesses of top/bottom Ag layer (5 nm thick) and DAST layer (60 nm thick).

MLMD layer (thickness)	Variation in thickness	BC mode			BW mode			DW mode		
		VT	IRT	SHGC	VT	IRT	SHGC	VT	IRT	SHGC
Top/Bottom Ag (5 nm)	Upper limit (+5%)	0.76	0.24	0.52	0.70	0.53	0.62	0.35	0.62	0.47
	Optimum dimension	**0.77**	**0.25**	**0.54**	**0.69**	**0.55**	**0.62**	**0.35**	**0.62**	**0.47**
	Lower limit (−5%)	0.79	0.26	0.55	0.69	0.56	0.63	0.35	0.62	0.48
DAST (60 nm)	Upper limit (+5%)	0.80	0.26	0.56	0.67	0.57	0.62	0.36	0.61	0.48
	Optimum dimension	**0.77**	**0.25**	**0.54**	**0.69**	**0.55**	**0.62**	**0.35**	**0.62**	**0.47**
	Lower limit (−5%)	0.74	0.24	0.51	0.72	0.53	0.63	0.34	0.63	0.47

Note: BC: Bright and Cool; BW: Bright and Warm; DW: Dark and Warm; VT: Visible Transmittance; IRT: IR Transmittance; SHGC: Solar Heat Gain Coefficient.

lithium niobate ($LiNbO_3$) or doped polymers may also be used, but they may require a very high voltage because of their small EO coefficients. Therefore, it is always desirable to look for more such EO materials that have certain optical absorption in the non-powered state to achieve different modes as per the requirement of the geographical location. Here, we emphasize that the temperature in the gap of an IGU of a window may exceed (90 °C) or even go below the freezing point in a few geographical places that face extreme weather conditions [45]. Therefore, it is equally important that EO material exhibits matched mechanical as well as thermal properties. This will ensure that its coefficient of thermal expansion closely matches with the metals used in the MLMD glasses, therefore, reducing the mechanical strain during expansion or cooling down. To have longevity and practical value, the EO material should also offer resistance to ultraviolet radiation, high humidity, exposure to direct sunlight, etc.

5. Conclusion

We proposed theoretical design of electrotunable smart glasses for dynamically controlling the amount of transmitted solar radiation depending upon the weather/climate condition. We explored noble metals as well as their relatively inexpensive alternatives as metallic layers. An electro-optic polymer is used as a dielectric layer to make the system tunable by using a bias voltage ranging from −15 V to +15 V. The figure-of-merit calculations show that our relatively inexpensive materials (Ag, Cu, ITO, AZO, and ALON) can outperform industry-standard commercial glasses and previously reported infrared-blocking plasmonic glasses. Our design is robust, low-cost, ultra-compact (60–100 nm thick), lithography-free, large-area compatible, polarization-independent, and angle-insensitive (up to 75 degrees). These ultra-thin smart glasses can be integrated into privacy windows, security panels, solar control skylight panels, etc. Aluminium oxynitride based glasses can be used in fighter aircraft, military vehicles, high security buildings, and submarine applications.

CRediT authorship contribution statement

Ashish K. Chowdhary: Conceptualization, Methodology, Software, Data Curation, Writing - original draft. **Debabrata Sikdar:** Visualization, Validation, Writing - review & editing, Supervision.

Declaration of competing interest

The authors declare that they have no known competing financial interests or personal relationships that could have appeared to influence the work reported in this paper.

References

[1] B. Ko, D. Lee, T. Badloe, J. Rho, Metamaterial-based radiative cooling: Towards energy-free all-day cooling, Energies 12 (1) (2018) 89.
[2] 2009 RECS survey data, consumption & expenditures (C&E) tables, 2020, https://www.eia.gov/consumption/residential/data/2009/index.php?view=consumption. (Accessed 29 May 2020).
[3] R. Farrington, J. Rugh, Impact of vehicle air-conditioning on fuel economy, tailpipe emissions, and electric vehicle range, 2020, http://www.nrel.gov/docs/fy00osti/28960.pdf. (Accessed 01 April 2020).
[4] R. Baetens, B.P. Jelle, A. Gustavsen, Properties, requirements and possibilities of smart windows for dynamic daylight and solar energy control in buildings: A state-of-the-art review, Sol. Energy Mater. Sol. Cells 94 (2) (2010) 87–105.
[5] F. Pacheco-Torgal, Eco-Efficient Materials for Mitigating Building Cooling Needs, Elsevier, Boston, 2015.
[6] J.A. Duffie, W.A. Beckman, Solar Engineering of Thermal Processes, John Wiley, Hoboken, 2013.
[7] M. Santamouris, Buildings, Energy, Solar Technology, Earthscan, London, 2007.
[8] J. Carmody, S. Selkowitz, L. Heschong, Residential Windows: A Guide to New Technologies and Energy Performance, New York, 1996.
[9] Seven sun windows - Insulating glasses, 2019, http://www.sevensunwindows.com/windows/replacement/glass. (Accessed 23 Nov 2019).
[10] Double-glazed, high-solar-gain low-E glass, 2020, https://www.efficientwindows.org/gtypes_2lowe.php. (Accessed 23 April 2020).
[11] L.V. Besteiro, X.T. Kong, Z. Wang, F. Rosei, A.O. Govorov, Plasmonic glasses and films based on alternative inexpensive materials for blocking infrared radiation, Nano Lett. 18 (5) (2018) 3147–3156.
[12] Z. Zhao, et al., Sn dopants improve the visible transmittance of VO2 films achieving excellent thermochromic performance for smart window, Sol. Energy Mater. Sol. Cells 209 (2020) 110443.
[13] H.D. Jeong, S.Y. Lee, Tunable plasmonic absorber using a nanoslit array patterned on a $Ge_2Sb_2Te_5$-inserted Fabry–Perot resonator, J. Lightwave Technol. 36 (2018) 5857–5862.
[14] M. Aalizadeh, A.E. Serebryannikov, A. Khavasi, G.A.E. Vandenbosch, E. Ozbay, Toward electrically tunable lithography-free ultra-thin color filters covering the whole visible spectrum, Sci. Rep. 8 (2018) 11316.
[15] J. Kim, M. Remond, D. Kim, H. Jang, E. Kim, Electrochromic conjugated polymers for multifunctional smart windows with integrative functionalities, Adv. Mater. Technol. 5 (2020) 1900890.
[16] Z. Wang, P. Zhou, G. Zheng, Electrically switchable highly efficient epsilon-near-zero metasurfaces absorber with broadband response, Results Phys. 14 (2019) 102376.
[17] A. Aoki, A. Ito, S. Watanabe, Reversible Ag electroplating onto ITO electrode for smart window, Sol. Energy Mater. Sol. Cells 200 (2019) 109922.
[18] W.J. Yoon, et al., A single-step dual stabilization of smart window by the formation of liquid crystal physical gels and the construction of liquid crystal chambers, Adv. Funct. Mater. 30 (2020) 1906780.
[19] M. Nejat, N. Nozhat, Design, theory, and circuit model of wideband, tunable and polarization-insensitive terahertz absorber based on graphene, IEEE Trans. Nanotechnol. 18 (2019) 684–690.
[20] S.S. Mirshafieyan, D.A. Gregory, Electrically tunable perfect light absorbers as color filters and modulators, Sci. Rep. 8 (2018) 2635.
[21] G. Wei, D. Yang, T. Zhang, X. Yue, F. Qiu, Thermal-responsive PNIPAm-acrylic/Ag NRs hybrid hydrogel with atmospheric window full-wavelength thermal management for smart windows, Sol. Energy Mater. Sol. Cells 206 (2020) 110336.
[22] Q. Gao, X. Wu, L. Cai, K.Dual.functionality. of, Dual functionality of $K_{0.3}WO_3/Ag_2O$ nanocomposites for smart window: Energy saving and visible photocatalytic self-cleaning performance, Sol. Energy Mater. Sol. Cells 196 (2019) 111–118.
[23] S. Haghanifar, T. Gao, R.T.R. De Vecchis, B. Pafchek, T.D.B. Jacobs, P.W. Leu, Ultrahigh-haze nanograss glass with fluid-induced switchable haze, Optica 4 (2017) 1522.

[24] A. Llordes, G. Garcia, J. Gazquez, D.J. Milliron, Tunable near-infrared and visible-light transmittance in nanocrystal-in-glass composites, Nature 500 (7462) (2013) 323–326.
[25] J. Pan, et al., A high-performance electrochromic device assembled with hexagonal WO_3 and NiO/PB composite nanosheet electrodes towards energy storage smart window, Sol. Energy Mater. Sol. Cells 207 (2020) 110337.
[26] B. Wang, et al., A long-life battery-type electrochromic window with remarkable energy storage ability, Sol. RRL 4 (2020) 1900425.
[27] R.J. Mortimer, D.R. Rosseinsky, P.M.S. Monk, Electrochromic Materials and Devices, John Wiley & Sons, 2015.
[28] Glass knowledge blog. Non-solar heat control glasses, 2019, https://theglassblog.wordpress.com/2011/02/06/non-solar-heat-control-glasses. (Accessed 23 Oct 2019).
[29] H. Weir, J.B. Edel, A.A. Kornyshev, D. Sikdar, Towards electrotuneable nanoplasmonic Fabry–Perot interferometer, Sci. Rep. 8 (2018) 565.
[30] D. Sikdar, A.A. Kornyshev, An electro-tunable Fabry–Perot interferometer based on dual mirror-on-mirror nanoplasmonic metamaterials, Nanophotonics 8 (12) (2019) 2279–2290.
[31] B.E.A. Saleh, M.C. Teich, Fundamentals of Photonics, Wiley, NY, 1991.
[32] A.K. Chowdhary, D. Sikdar, Ultra-broadband wide-angle metallo-dielectric metamaterial absorber for solar energy harvesting, in: 2019 Workshop on Recent Advances in Photonics, WRAP, 2019, pp. 1–3.
[33] E. Hecht, Optics, Addison–Wesley, New York, 2002.
[34] P.B. Johnson, R.W. Christy, Optical constants of the noble metals, Phys. Rev. B 6 (12) (1972) 4370.
[35] H. Zheng, et al., Optical properties of Al-doped ZnO films in the infrared region and their absorption applications, Nanoscale Res Lett. 13 (2018) 149.
[36] T.M. Hartnett, S.D. Bernstein, E.A. Maguire, R.W. Tustison, Optical properties of ALON (aluminum oxynitride), Proc. SPIE 3060 (1997) 284–295.
[37] D.M. Pozar, Microwave Engineering, Wiley, Hoboken, NJ, 2005.
[38] S.O. Kasap, Optoelectronics and Photonics: Principles and Practices, 2013.
[39] W. Geis, R. Sinta, W. Mowers, S.J. Deneault, M.F. Marchant, K.E. Krohn, S.J. Spector, D.R. Calawa, T.M. Lyszczarz, Fabrication of crystalline organic waveguides with an exceptionally large electro-optic coefficient, Appl. Phys. Lett. 84 (2004) 3729–3731.
[40] M. Ramisetty, S. Sastri, U. Kashalikar, L.M. Goldman, N. Nag, Transparent poly-crystalline spinels protect and defend, Am. Ceram. Soc. Bull. 92 (2013) 20–24.
[41] Domes & infrared optics, Surmet, 2020, http://www.surmet.com/products-and-applications/Domes-and-IR-Optics. (Accessed 02 Mar 2020).
[42] Z.Y. Li, S. Butun, K. Aydin, Large-area, lithography-free super absorbers and color filters at visible frequencies using ultrathin metallic films, ACS Photonics 2 (2015) 183–188.
[43] J. Park, J.H. Kang, X.G. Liu, M.L. Brongersma, Electrically tunable epsilon-near-zero (ENZ) metafilm absorbers, Sci. Rep. 5 (2015) 15754.
[44] K. Lee, S.Y. Han, Z. Li, H.W. Baac, H.J. Park, Flexible high-color-purity structural color filters based on a higher-order optical resonance suppression, Sci. Rep. 9 (2019) 14917.
[45] Z. Respondek, Heat transfer through insulating glass units subjected to climatic loads, Materials 13 (2) (2020) 286.